



Research  
Textile Engineering—Article

# Freezing-Extraction/Vacuum-Drying Method for Robust and Fatigue-Resistant Polyimide Fibrous Aerogels and Their Composites with Enhanced Fire Retardancy



Kaiqing Yao<sup>a</sup>, Chonghu Song<sup>a</sup>, Hong Fang<sup>a</sup>, Feng Wang<sup>b</sup>, Lian Chen<sup>b</sup>, Shaohua Jiang<sup>b,\*</sup>, Guojun Zha<sup>c</sup>, Haoqing Hou<sup>a,\*</sup>

<sup>a</sup> Department of Chemistry and Chemical Engineering, Jiangxi Normal University, Nanchang 330022, China

<sup>b</sup> Jiangsu Co-Innovation Center of Efficient Processing and Utilization of Forest Resources, International Innovation Center for Forest Chemicals and Materials, College of Materials Science and Engineering, Nanjing Forestry University, Nanjing 210037, China

<sup>c</sup> School of New Energy Science and Engineering, Xinyu University, Xinyu 330020, China

## ARTICLE INFO

### Article history:

Received 23 February 2021

Revised 12 June 2021

Accepted 24 August 2021

Available online 10 December 2021

### Keywords:

Polyimide aerogel  
Freeze-extraction  
Vacuum-drying  
Mechanical property  
Thermal insulation  
Fire retardancy

## ABSTRACT

In the rapid development of modern materials, there is a great need for novel energy-saving, time-saving, cost-saving, and facile approaches to fabricate light, low-density, and high-porosity aerogels with excellent mechanical and thermal performance. In this work, a freeze-extraction method combined with normal vacuum-drying (VD), using short electrospun polyimide (PI) fibers as a supporting skeleton, was developed to prepare high-performance PI fibrous aerogels (PIFAs) without the need for a special drying process. The resulting PIFAs exhibit low density ( $\leq 52.8 \text{ mg}\cdot\text{cm}^{-3}$ ) and high porosity ( $> 96\%$ ). The PIFAs are highly fatigue resistant, with cycling compression for at least 20 000 cycles and a low energy-loss coefficient. A thermal conductivity of  $40.4 \text{ mW}\cdot\text{m}^{-1}\cdot\text{K}^{-1}$  was obtained for a PIFA with a density of  $39.1 \text{ mg}\cdot\text{cm}^{-3}$ . Further modification of the PIFAs with polysilazane led to enhanced fire resistance and a high residue ( $> 70\%$ ) in a nitrogen atmosphere. These excellent properties make PIFAs and their composites promising candidates for lightweight construction, thermal insulating, and fireproof layers for the construction industry, aviation, and aerospace industries, as well as for high-temperature reaction catalyst carriers. In addition, the proposed freezing-extraction/VD approach can be extended to other material systems to provide savings in energy, time, and costs.

© 2021 THE AUTHORS. Published by Elsevier LTD on behalf of Chinese Academy of Engineering and Higher Education Press Limited Company. This is an open access article under the CC BY-NC-ND license (<http://creativecommons.org/licenses/by-nc-nd/4.0/>).

## 1. Introduction

Aerogels are typical three-dimensional (3D) porous materials that have attracted a great deal of attention due to their excellent properties and broad applications [1,2]. In recent years, 3D fibrous aerogels made from fibers with extraordinary properties have drawn a tremendous amount of attention due to their superior characteristics, which include interconnected networks, low density, high porosity, high surface area, and low thermal conductivity [3–6]. Therefore, such 3D fibrous aerogels, which are also known as “sponges,” are ideal candidates for applications in the field of thermal insulation [7,8], solvent absorption [9], oil absorption/separa-

tion [10–12], cell culture [13], stimuli-responsive devices [14,15], electromagnetic shielding [16,17], water remediation [18], and particle filters [19,20]. In particular, among the various 3D electrospun polymeric aerogels that have been reported in the literature, electrospun polyimide fibrous aerogels (PIFAs) have attracted considerable attention due to their thermal insulation, high porosity, and excellent mechanical properties [8,21–23].

Polyimide (PI)-based aerogels can be fabricated using either freeze-drying (FD) or supercritical drying (SD) methods [8,24–27]. FD and SD techniques can effectively restrain the collapse of the pore structure during drying [28–32]. However, both techniques require sophisticated instruments to create either ultralow temperatures under vacuum conditions or high temperatures in ultrahigh-pressure environments. In addition, their time-consuming, costly, low-producing, and scale-restricted drying processes are fatal flaws that hinder further practical applications of

\* Corresponding authors.

E-mail addresses: [shaohua.jiang@njfu.edu.cn](mailto:shaohua.jiang@njfu.edu.cn) (S. Jiang), [haoqing@jxnu.edu.cn](mailto:haoqing@jxnu.edu.cn) (H. Hou).

FD and SD techniques, especially for large-scale production. Convenient and inexpensive large-scale preparation is crucial for practical applications to be possible for such techniques. Compared with traditional drying methods, vacuum-drying (VD), which does not require special facilities, is both time-saving and convenient. In the literature, the VD technique has been applied to prepare several polymer-based aerogels. A bridged silsesquioxane aerogel prepared by VD showed a compressive modulus of 139.2 kPa with a density of  $85 \text{ mg}\cdot\text{cm}^{-3}$  at 60% strain [33]. Yet only 20 cycles of the loading–unloading process were conducted at 30% strain, and too much alcohol was consumed during the drying process of this organic silicon aerogel. Li et al. [34] reported a reduced graphene oxide (GO) aerogel prepared by a VD/ambient drying method, which exhibited a compressive stress of 0.019 MPa and a density of  $5.3 \text{ mg}\cdot\text{cm}^{-3}$ . However, the graphene aerogel reported in that work had an energy-loss coefficient greater than 50% and a degradation of compressive strength of over 20% after only 10 cycles of compressive work. These weak mechanical properties probably originate from the rather low concentration and disorder of the GO lamella in the precursor dispersion. A phenolic polymer-derived carbon aerogel for use in organic solvents absorption was prepared through VD, and exhibited a low density of  $25 \text{ mg}\cdot\text{cm}^{-3}$  [35]. Nonetheless, the method introduced in that work is only appropriate for producing phenolic polymer-derived carbon aerogels, rather than neat polymer aerogels. Plus, the health issues that have been reported with the use of  $\text{ZnCl}_2$  limits its application. PI aerogels made using VD after a sol–gel and solvothermal imidization process have been reported [36,37]. However, these kinds of PI aerogels show relatively weak mechanical properties at relatively high densities. For example, using aromatic dianhydrides and triamines as monomers, PI aerogels prepared by means of the sol–gel followed by hydrothermal imidization process and then VD, exhibited a density greater than  $140 \text{ mg}\cdot\text{cm}^{-3}$  but a maximum stress of 95% and 87% after only 10 cycles of the loading–unloading process. The relatively poor fatigue resistance and structural stability of these PI aerogels mainly resulted from the low molecular weight of the poly(amic acid) (PAA) used in that work, in comparison with the PAA synthesized from dianhydrides and diamines. Furthermore, a solvothermal imidization process that is maintained for over 10 h is harmful to the structural stability of the PAA precursor gels in an atmosphere with high temperature and pressure. Therefore, a novel energy-, time-, and cost-saving method is greatly required for the preparation of high-performance PIFAs.

In this research, we highlight a strategy involving freeze-extraction followed by VD to fabricate PIFAs using short PI fibers as a skeleton. Strengthening the initial framework stiffness of the precursor aerogel and reducing the capillary pressure caused by solvent evaporation resulted in no obvious volume shrinkage or structural cracking being observed during the entire VD process. The obtained vacuum-dried aerogels exhibited excellent mechanical performance, superior thermal insulation, and low thermal conductivity. Further modification by polysilazane significantly enhanced the thermal properties and fire retardancy of the composite aerogels.

## 2. Experimental section

### 2.1. Materials

Electrospun short PI fibers from monomers of pyromellitic dianhydride (PMDA) and 4,4'-oxydianiline (ODA) with an average length of 1 mm were provided by Jiangxi Xiancai Nanofibers Technology Co., Ltd., China. ODA (Changzhou Sunlight Pharmaceutical Co.) and 3,3',4,4'-biphenyltetracarboxylic dianhydride (BPDA;

Changzhou Sunlight Pharmaceutical Co.) were purified by sublimation before use. *N,N*-dimethylacetamide (DMAc; 99%; Shanghai Chemical Reagents Co., China) was purified by distillation before use. Triethylamine (TEA; 99%; Tianjin Zhiyuan Chemicals Co., Ltd., China), formic acid (88%; Tianjin Zhiyuan Chemicals Co., Ltd., China), tetrahydrofuran (THF; 99%; Tianjin Zhiyuan Chemicals Co., Ltd.), and polysilazane (Anhui Lota Silicon Oil Co., Ltd., China) were used as received without further purification.

### 2.2. Preparation of PAA

In brief, equal molar ratios of BPDA and ODA were reacted in DMAc at 0 °C for 24 h, followed by a partial amination process with a 60% molar ratio to BPDA of TEA. After stirring for 0.5 h, the obtained solution (6.2 wt%) was stored in the refrigerator for future use.

### 2.3. Preparation of PIFAs

In a typical experiment, 1.02 g of short PI fibers (1 mm) were mixed with 16.45 g of diluted partially aminated PAA solution with 35.57 g of DMAc and 0.71 g of deionized water (2 wt% weight ratio to DMAc). The prepared dispersion was transferred into an aluminum foil pan and frozen in liquid nitrogen until the dispersion transformed into a solid, which was then slowly immersed in a non-solvent (water/ethanol/formic acid, 70:30:10, v/v/v) with stirring ( $500 \text{ r}\cdot\text{min}^{-1}$ ) to accelerate the solvent-extraction process. The whole solvent-extraction process took approximately 3 h for a sample with a thickness of 1.8–2.2 cm and 1.5 h for a sample with a thickness of 0.8–1.2 cm. When the freeze-extraction process was complete, the porous and rigid wet aerogel was washed with ethanol, followed by VD at 120 °C for 2 h. After the VD process, the precursor aerogel was heated to 300 °C ( $2 \text{ }^\circ\text{C}\cdot\text{min}^{-1}$ ) and annealed for 1 h under a nitrogen atmosphere to implement the imidization process. Depending on the solid contents of the PAA solutions, the as-prepared PIFAs were denoted as PIFA-1.4, PIFA-1.6, PIFA-1.8, and PIFA-2.0, with densities of 39.1, 42.4, 46.7, and  $52.8 \text{ mg}\cdot\text{cm}^{-3}$ , respectively. The mass of the aerogels was measured using an analytical balance; the volume was determined by the length, width, and height of the rectangular samples; and the density (mass/volume) of the aerogels was then obtained.

### 2.4. Preparation of polysilazane-modified PIFAs

The PIFAs were immersed in a polysilazane tetrahydrofuran solution (2 wt%) and squeezed to facilitate the absorption process. This was followed by air drying at 80 °C to obtain polysilazane-modified PI fibrous aerogels (PszmPIFAs). The PszmPIFAs were further heated at 180 °C for 2 h and at 430 °C under a nitrogen atmosphere for 1 h to cure the polysilazane. The PIFAs that were modified following this protocol once, twice, and three times were denoted as PszmPIFAs1, PszmPIFAs2, and PszmPIFAs3, respectively.

### 2.5. Characterization

A scanning electron microscope (SEM; VEGA 3 SBU; TESCAN, Czech Republic) was used to observe the morphologies of the PI fibers and the aerogel samples. Compression tests and cyclic compression tests were performed on a compression tester (CMT8202; SANS, China) at a compression rate of  $50 \text{ mm}\cdot\text{min}^{-1}$ . Tests with 20 000 compression cycles were conducted, and the plots for the 1st, 20th, 200th, 2000th, and 20 000th cycles were recorded. Transmission electron microscopy (TEM; Titan G2 60-300; FEI, USA) was used to observe the morphologies of the PszmPIFAs. Thermogravimetric analysis (TGA) was performed on a TGA-55 (TA Instru-

ments, USA) under a nitrogen atmosphere with a heating rate of  $10\text{ }^{\circ}\text{C}\cdot\text{min}^{-1}$  from 50 to  $800\text{ }^{\circ}\text{C}$ . Thermal conductivity was measured using a Hot Disk thermal constants analyzer (TPS 2500S; Hot Disk, Sweden) with a Kapton sensor (5465; Hot Disk). The density of the aerogels was calculated by  $(1 - \rho_0/\rho_{\text{bulk}}) \times 100\%$ , where  $\rho_0$  the apparent density of the aerogel and  $\rho_{\text{bulk}} = 1.4\text{ g}\cdot\text{cm}^{-3}$  is the density of PI in the bulk state. A Quantachrome Autosorb IQ2 automatic adsorption/desorption analyzer (USA) was used to measure specific surface areas, as well as the pore size and distribution of the aerogel materials.

### 3. Results and discussion

#### 3.1. Fabrication of PIFAs and PsmPIFAs

The concept for the preparation of the PIFAs and PsmPIFAs is schematically shown in Fig. 1. In general, short PI fibers can be obtained by continuous electrospinning, thermal imidization, and pulverizing. However, the short PI fibers that are obtained by pulverizing PI nonwovens possess uneven fiber length and aspect ratios, which affect the pore structures and mechanical performance of the resultant PIFAs. In this work, the short fibers were provided by Jiangxi Xiancai Nanofibers Technology Co., Ltd., China. As shown in Fig. S1 in Appendix A, the short PI fibers possessed a homogeneous size, with an average length of about 1 mm and diameter of about  $1.2\text{ }\mu\text{m}$ . These short PI fibers were then mixed with PAA to form a homogenous, viscous, and stable suspension, in which the PI fibers could be dispersed well and bonded by PAA via a “self-gluing” mechanism [8,23]. To be precise, because the PAA can be thermally imidized further, the additional PAA acted as a glue on the short PI fibers, which were then converted into PI, and finally formed a composite structure with the PI resin self-gluing the short PI fibers. It was notable that the minor addition of water as a solvent increased the surface tension of the solvent, thereby restraining the volume shrinkage upon freezing [3].

It is also notable that special drying methods were not required in this case because a cellular structure had already formed after the non-solvent phase separation induced by the non-solvent exchange. In this method, large pores formed in the outer parts of the aerogels due to the expansion of ice and solvent exchange. The formation of a porous structure before drying facilitated the elimination of polar solvents [34,38,39]. Moreover, the robust precursors of the PIFAs were able to withstand the capillary forces originating from the polar solvents, which allowed the drying process to be conducted in an ordinary vacuum oven while maintaining the porous structure [35,38–41].

In general, the freeze-extraction/VD preparation process used in this work saves energy, time, and costs. First, the raw PI fibers used in this work were commercially provided by Jiangxi Xiancai Nanofibers Technology Co., Ltd., China, and were thus much

cheaper than lab-made PI fibers. In addition, the devices used in this work are much cheaper than specialized machines such as freeze-driers and supercritical driers. In order to prepare samples with the same size, such as  $0.09\text{ m}^2$ , traditional FD and SD processes require a freeze drier (850 W, LC-10 N-50B; Shanghai Lichen Bangxi Instrument Technology Co., Ltd., China) or a supercritical drier (12 kW, SFE-02; Nantong Yichuang Experimental Instrument Co., Ltd., China) to be operating for at least 48 h. In contrast, the VD process used in this work only requires a normal vacuum oven (300 W, DZF-6020A; Shanghai Lichen Bangxi Instrument Technology Co., Ltd.) operating for around 10 h, which saves both energy and time in comparison with the other two techniques.

#### 3.2. The hierarchical cellular structure of PIFAs

It was observed that the higher solid content of the PAA was, the more visible was the honeycomb structure of the aerogels from PIFA-1.4 to PIFA-2.0 because continuous porous solid phases were more likely to form as the solid content of the PAA increased (Figs. 2 (a–d)). Cross-sectional SEM images of PIFA-2.0 are shown in Figs. 2 (d–f). This aerogel exhibited a dual pore structure with major pores (i.e., pores formed by non-solvent-induced phase separation during the freeze-extraction process) and minor pores (i.e., pores between the fibers). The aerogel exhibited an open-cellular architecture with interconnected pores through triangular junctions and a major cellular pore size of  $70\text{--}80\text{ }\mu\text{m}$ . The fibrous cell walls consisted of minor pores constructed by overlaid short PI fibers. Simultaneously, PI aggregated on the short fibers and acted as a glue, reinforcing the mechanical properties of the aerogel [42].

It is well known that thermal treatment induces significant volume shrinkage in PI aerogels due to thermal shock stress during thermal treatment. Nevertheless, with an increase in the mass ratio of fibers to PAA, the PIFA shrinkage decreased from 29.5% to 19.2%, indicating that the structural stability of the PIFAs clearly improved. The shrinkage of the PIFAs prepared by the freeze-extraction method was comparable to or even better than that of PIFAs prepared using FD, and lower than the shrinkage of PIFAs prepared using the SD method [43–46]. With an increase in the amount of PAA, an escalating trend was observed in the apparent density of the PIFAs, ranging from  $39.1\text{ mg}\cdot\text{cm}^{-3}$  (PIFA-1.4) to  $52.8\text{ mg}\cdot\text{cm}^{-3}$  (PIFA-2.0) (Fig. 2(g)). Although shrinkage occurred during the thermal imidization process, the porosities of the PIFAs were greater than 96.0% (96.2%–97.2%) (Fig. 2(h)).

As shown in Fig. 3(a), the obtained specific surface areas of the PIFAs were in the range of  $2\text{--}4\text{ mL}\cdot\text{g}^{-1}$ , which coincides with the values for other porous materials [9,23]. Fig. 3(b) demonstrates the existence of a bimodal porous structure in the PIFAs. The pore sizes were mainly distributed within the ranges of  $3\text{--}27$  and  $60\text{--}80\text{ }\mu\text{m}$ , respectively. The small pores were derived from the spaces

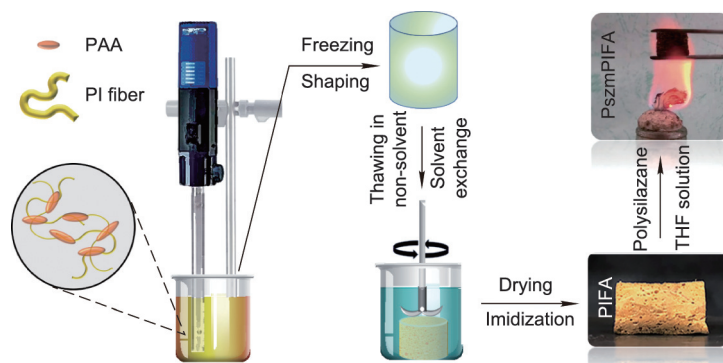


Fig. 1. Structural design and process used to make PIFA and PsmPIFA.

between the entangled fibers, while the big pores resulted from the non-solvent-induced phase separation during the freeze-extraction process. The porous characteristics shown in Fig. 3 agree well with the SEM results shown in Fig. 2.

### 3.3. Mechanical properties of PIFAs

The compressive properties of the PIFAs are shown in Fig. 4. It was found that the maximum stress of the PIFAs gradually

increased from 49 to 189 kPa as the loading amount of PAA increased (Fig. 4(a)). Due to the good compression resistance, the resulting PIFAs could withstand a weight of 200 g (581 times greater than the weight of the PIFAs themselves) without obvious deformation and a weight of 2 kg without any fracture (see insets of Fig. 4(a)). The stress–strain ( $\sigma$ – $\epsilon$ ) curves for PIFA-2.0 at various maximum compression strains of 20%, 30%, 40%, 50%, and 60%, with the stress ranging from 12 to 211 kPa, are presented in Fig. 4(b). It should be noted that, in applications, a monolithic PI

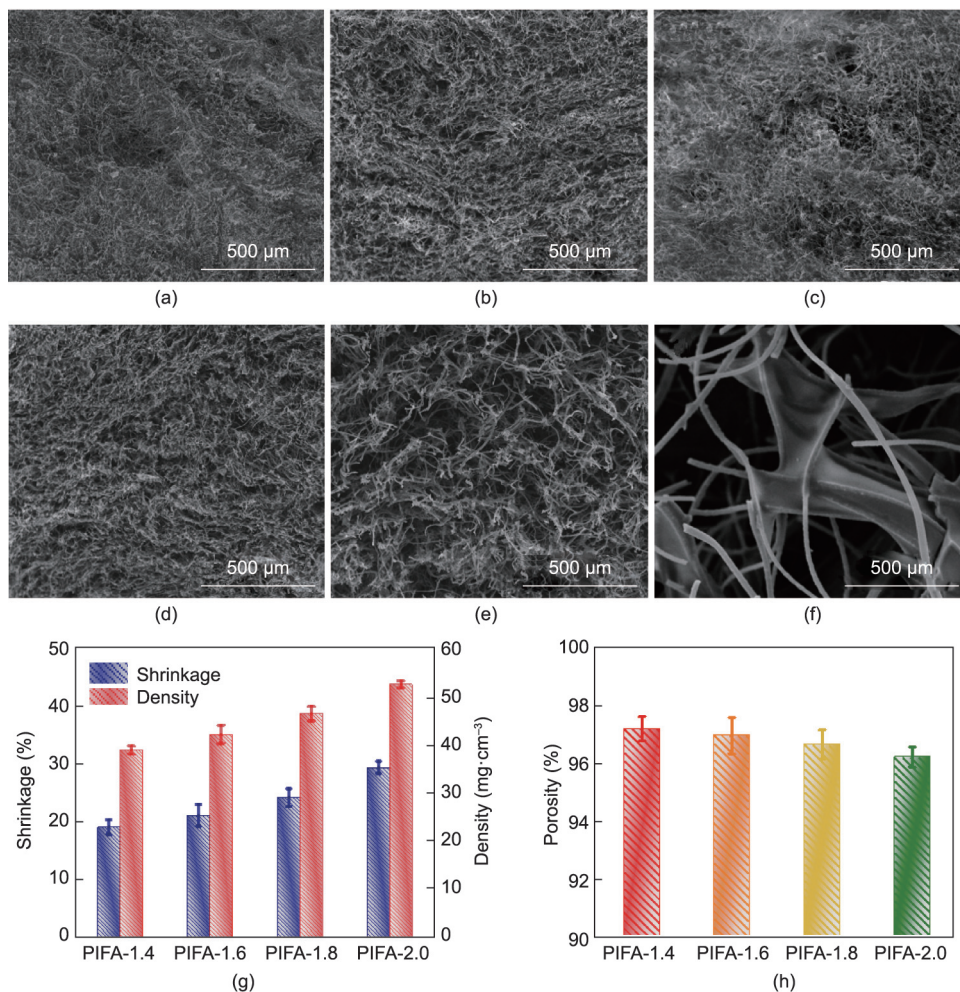


Fig. 2. Microstructures and structural formability of PIFAs. (a–c) SEM cross-sectional images of PIFA-1.4, PIFA-1.6, and PIFA-1.8; (d–f) SEM cross-sectional images of PIFA-2.0 under different magnifications; (g) shrinkage rates and density of PIFAs; (h) porosity of PIFAs.

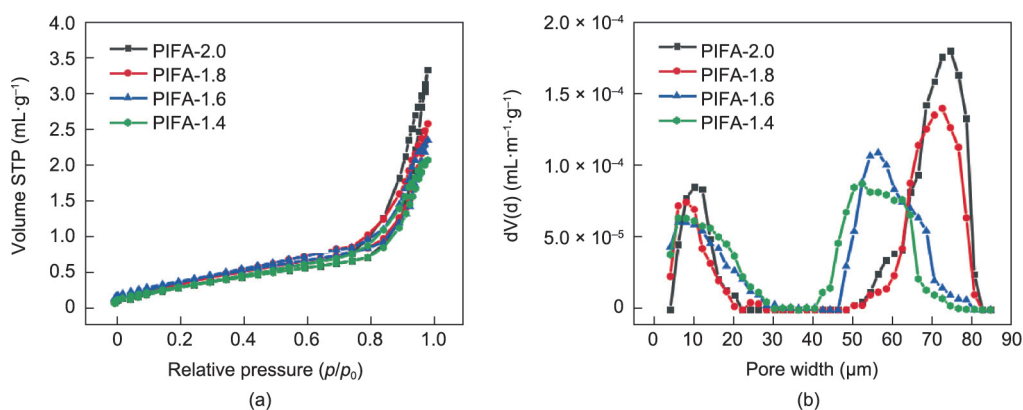
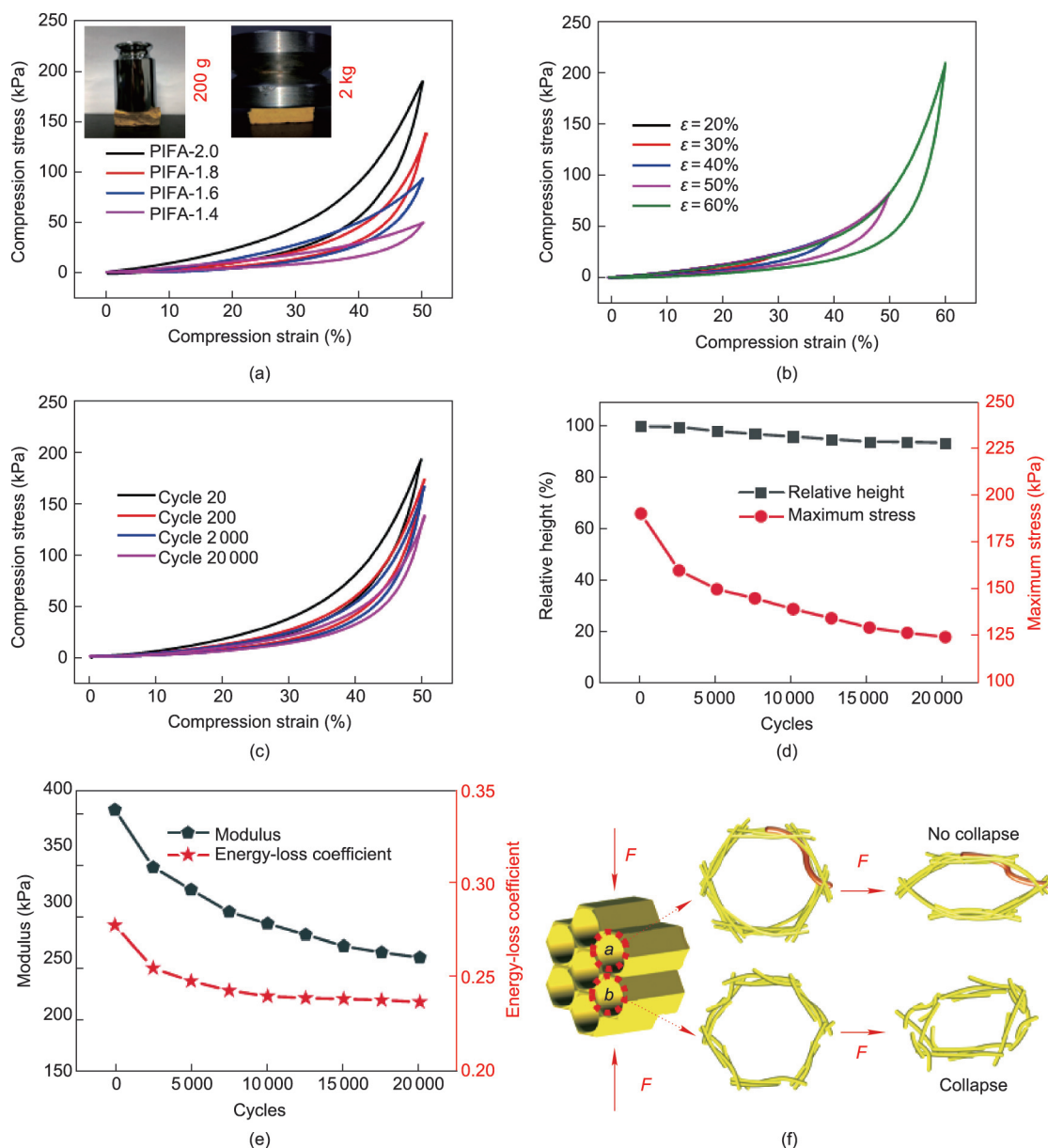


Fig. 3. (a) Nitrogen adsorption–desorption isotherm; and (b) pore size distributions of the PIFAs. STP: standard atmospheric pressure; dV(d): pore diameters.



**Fig. 4.** The multicycle compressive properties of PIFAs. (a) Stress–strain plots of PIFAs for the first cycle; (b) stress–strain plots during loading–unloading processes with different levels of compression strains; (c) stress–strain plots for different compression cycles at a compressive strain of 50%; (d) relative height evolution and maximum stress after different compression cycles; (e) Young’s modulus and energy-loss coefficient as functions of compressive cycles; (f) sketch of the bending of fibrous cell walls under compression. *F*: the force imposed on the pore structures; *a*: the pore structure containing a high aspect ratio and rough PI fibers; *b*: the pore structure containing mere small aspect ratio PI fiber.

aerogel requires an outstanding compressive fatigue resistance. Therefore, the compressive fatigue durability of the PIFAs (taking PIFA-2.0 as an example) was evaluated by conducting a compression cycling test of at least 20 000 loading–unloading cycles at a compression strain of 50% (Fig. 4(c)). Remarkably, PIFA-2.0 maintained 94% of its initial height, demonstrating only a negligible plastic deformation of 6.33% at 50% compression, even after 20 000 cycles, thus further highlighting the excellent fatigue resistance of the PIFAs (Fig. 4(d)). Although the maximum stress of PIFA-2.0 decreased from 189 to 125 kPa during the whole compressive test, the PIFA still retained over 66% of its initial strength, thereby demonstrating its durable cycling performance and structural stability. The variation of the Young’s modulus, which decreased from 378 to 250 kPa, was the same as that of the compressive strength. We estimated the work performed in the com-

pression (*U*) and the energy dissipation ( $\Delta U$ ), which could be determined from the hysteresis loops between the loading and unloading curves, yielding energy-loss coefficients ( $\Delta U/U$ ) (Fig. 4(e)). The energy-loss coefficient of PIFA-2.0 decreased from 0.27 for the first cycle to 0.26 for the 2500th cycle, and then remained at 0.24 for subsequent cycles (Fig. 4(e)). The energy-loss coefficient of the PIFAs in this work is smaller than those reported for other aerogels [7,47–49].

It is common for fibers with high aspect ratios (length/diameter) to possess a great deal of contact and to entangle and twist with each other, increasing the interactions among them [50]. The PI fibers used in this work had a length of about 1 mm and a diameter of about 1.2  $\mu\text{m}$ , with a large aspect ratio of 833, so they possessed the flexibility to entangle and twist with each other. Such a high aspect ratio resulted in much better fatigue resistance than the

PIFAs reported in our previous work [8,23]. As illustrated in Fig. 4(f), the cell walls fabricated by PI fibers with a small aspect ratio are discontinuous, fragile, and flexible, with a tendency to collapse and insufficient ability to recover, caused by bending-dominated buckling. In contrast, in a honeycomb structure, the cell walls fabricated by well-bonded and highly tangled PI fibers with a high aspect ratio possess a more robust and continuous structural support, which is beneficial for transferring the loading stress along the fibers—an essential part of elastic recovery. Furthermore, rough PI fibers serve as strong pillars and beams in the cell walls when such fibers are added, further strengthening the resilience of the honeycomb structure [7,13]. Using this method, lightweight PIFAs, which are 3D polyimide materials, can easily be prepared and possess both elasticity and excellent fatigue resistance, compared with the values reported in the literature so far (Table S1 in Appendix A).

### 3.4. Thermal insulation performance of PIFAs

Aerogels are most commonly used thermal insulation materials due to their low thermal conductivity, which stems from their high porosity. Because of their low solid fraction and high porosity, PIFAs prepared by the solvent-extraction method exhibit low thermal conductivity. Created by interconnected networks, tortuous porous paths result in low solid thermal transportation. Furthermore, the intertwined networks decrease the gas thermal conductivity of PIFAs by extending the flow space of air molecules. As shown in Fig. 5(a), as the density of PIFAs decreased, the thermal conductivity ( $\lambda$ ) slightly decreased. Notably, the thermal conductivity of PIFA-1.4, PIFA-1.6, PIFA-1.8, and PIFA-2.0 was 40.4, 42.2, 42.8, and 44.0  $\text{mW}\cdot\text{m}^{-1}\cdot\text{K}^{-1}$ , respectively. As shown in Fig. 5(b), PIFAs (taking PIFA-2.0 as an example) exhibited a low conductivity

( $44.0 \text{ mW}\cdot\text{m}^{-1}\cdot\text{K}^{-1}$ ), which is comparable with those of other reported aerogels and sponges, including PI/rGO/Co aerogel [51], polybenzazole aerogel [47], PI fiber assembled sponge prepared by FD [8],  $\text{SiO}_2\text{-Al}_2\text{O}_3$  composite ceramic sponge [49], silver nanowires/PI sponge [52], and bamboo fiber-modified foam [53]. Furthermore, the PIFAs outperformed wood aerogels [48] in terms of low conductivity. It can be seen from Fig. 5(b) that the PIFAs in this work possessed both a low energy-loss coefficient at a large compressive strain and low thermal conductivity. These performances are promising for practical thermal insulation applications. We further observed the dynamic temperature distribution of PIFA-2.0 by means of infrared camera by heating the PIFA on a  $350^\circ\text{C}$  platform for 30 min. As shown in Fig. 5(c), it was observed that a gradient temperature was distributed from the interface between the platform and the bottom of the sample through to the top of the sample. The temperature of the top surface of PIFA-2.0 (22 mm thick) remained at about  $55.0^\circ\text{C}$  for 1 min; it then increased to  $65.0^\circ\text{C}$  after 10 min of heating and subsequently remained near  $75.0^\circ\text{C}$  after 20 min. After being removed from the  $350.0^\circ\text{C}$  platform for 5 s, the temperature at the bottom and top surfaces dropped to  $221.2$  and  $45.7^\circ\text{C}$ , respectively, which made it possible to pick up the PIFA from the top with a bare hand (Fig. 5(d)). These results demonstrate the PIFA's excellent performance as a thermal insulator against a high temperature over a long period of time.

### 3.5. Polysilazane-modified PIFAs

PI aerogels have great potential for use as lightweight fire-retardant materials. Adding inorganic fillers can be an effective strategy to improve their fire resistance [54,55]. However, the addition of such fillers also results in the sacrifice of mechanical

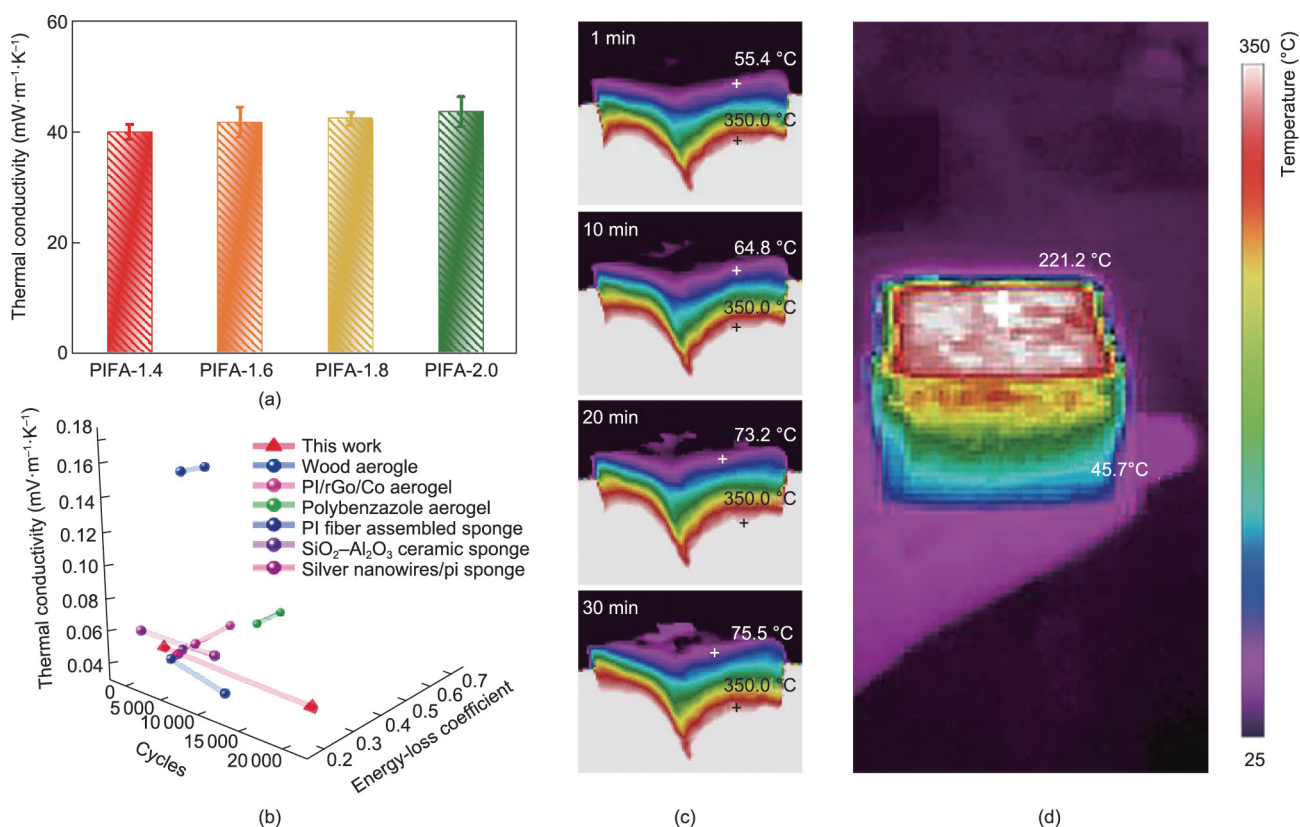


Fig. 5. Thermal insulation properties of the PIFAs. (a) Thermal conductivity of the PIFAs; (b) thermal conductivity and energy-loss efficient of PIFA-2.0, as compared with those of aerogel-like materials reported in the literature; (c) infrared images of PIFAs on a  $350^\circ\text{C}$  heating platform for 30 min; (d) a hand holding the PIFA after it had been heated on a  $350^\circ\text{C}$  platform.

flexibility and a significant increase in density. Therefore, it would be better to modify PI aerogels with inorganic polymer materials, which possess more tenacity than inorganic particles. Herein, we developed a facile method to modify PIFAs through the adsorption of polysilazane solution followed by air drying. Polysilazane, a Si–N-containing inorganic polymer with high polarity, possesses good adhesion to different surfaces [56]. Therefore, it can easily form a coating on PI nanofibers (PINFs). After further thermal treatment at a high temperature, the polysilazane coating can be self-crosslinked into a more stable compound to bind the PINFs [57].

As displayed in Fig. 6(a), the PI fibers of the PIFAs were wrapped and adhered by a layer of polysilazane. An ultrathin layer of polysilazane with a thickness of 42 nm was coated onto the PI fibers, as shown in the selected-area TEM image, serving as a glue to bind the PI fibers together (Fig. 6(b)). According to energy dispersive spectrometer (EDS) mapping of the cross-section, the PsmPIFA2 contained elements of carbon (C), nitrogen (N), oxygen (O), and silicon (Si), with the Si element deriving from the polysilazane and all elements being homogeneously distributed (Figs. 6(c–h)).

### 3.6. Thermal and mechanical behavior of PsmPIFAs

The thermal properties of the PIFAs and PsmPIFAs were investigated by means of TGA (Fig. 7(a)). All the samples were found to be thermally stable until 300 °C. The PIFAs started to decompose at around 350 °C, with weight loss that can be attributed to the release of CO<sub>2</sub> and H<sub>2</sub>O to form residual carbon. In comparison, the PsmPIFA samples started to decompose at around 450 °C, with weight loss coming from the decomposition of PIFA to form residual carbon and the decomposition of polysilazane to form SiN<sub>4</sub> [58]. The PsmPIFAs exhibited a decomposition temperature

100 °C higher than that of the PIFAs. PsmPIFAs that had been modified with polysilazane once, twice, and three times had residues of 68.2%, 76.1%, and 78.5%, respectively, which were much higher than that of PIFAs (60.4%). Fig. 7(b) presents the weight loss of PI-based aerogels versus their burning time curves. During the combustion process, PsmPIFA1, PsmPIFA2, and PsmPIFA3 preserved 66.9%, 73.9%, and 77.5% of their original weight, respectively, when exposed to a high-temperature flame for 60 s. These values were clearly higher than that of PIFA-2.0, revealing that the PsmPIFAs possessed much better flame retardancy than the PIFAs, probably due to the coating of polysilazane. The polysilazane coating forms a gas barrier around the PIFAs to separate the sample from oxygen, and thus prevents the generation of fire. In addition, during the burning, the polysilazane thermally decomposes into inorganic Si–O–Si bonds under an oxygen atmosphere [59], which further protects the PIFAs from burning and enhances the flame retardancy of the PsmPIFAs.

To our surprise, polysilazane not only improved the combustion behavior, but also decreased the thermal conductivity of the PIFAs. Compared with PIFA-2.0, a lower conductivity of 38.5 mW·m<sup>-1</sup>·K<sup>-1</sup> was achieved from sample PsmPIFA1 (Fig. 7(c)). With an increased loading of polysilazane, the conductivity of PsmPIFA2 further decreased to 36.4 mW·m<sup>-1</sup>·K<sup>-1</sup>. More intuitively, the dynamic temperature distribution of PsmPIFA2 was observed using the same method as that used for PIFA-2.0 (Fig. 7(d)). It was observed that the temperature of the top surface of PsmPIFA2 slowly increased from 45.9 to 68.8 °C in 30 min; furthermore, PsmPIFA2 maintained lower temperatures than those of PIFA-2.0 during the whole high-temperature heating process, indicating that modification with polysilazane effectively reduced the thermal conductivity of the PIFAs.

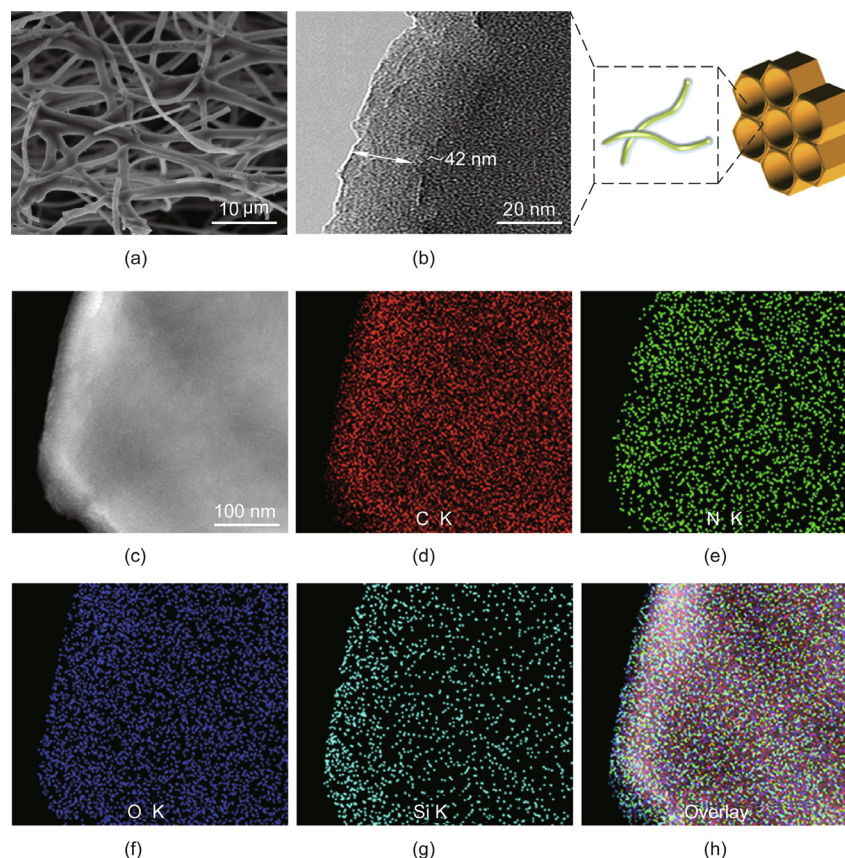


**Fig. 6.** Representative graphs of PsmPIFAs. (a) SEM image of the cell wall of PsmPIFA2; (b) schematic and TEM images of the selected region at the edge of a PsmPIFA; (c–h) TEM and energy dispersive spectrometer (EDS) mapping spectrum images of the selected region at the edge of a PsmPIFA. K: the K shell of atom.

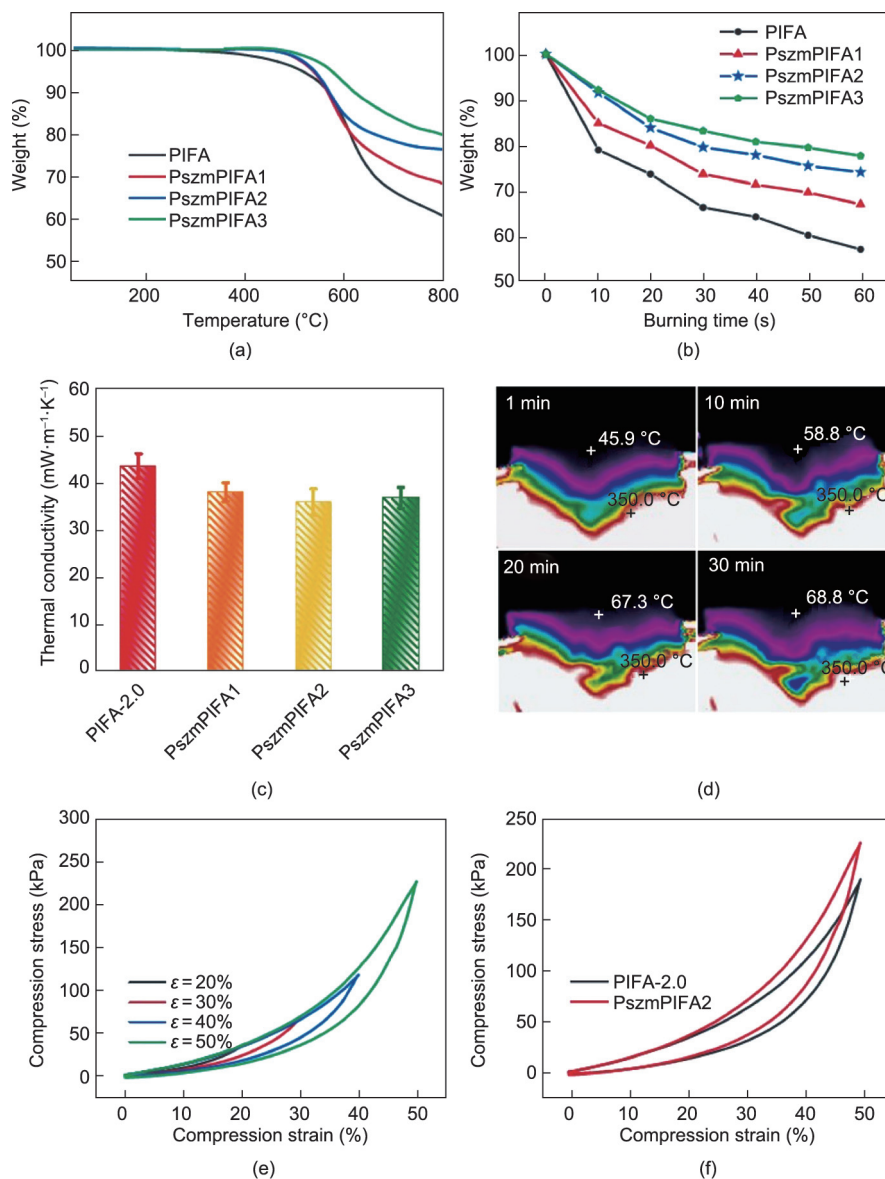


**Fig. 7.** Thermal insulation properties and mechanical performance of PszmPIFAs. (a) TGA curves of PI-based aerogels; (b) weight loss versus burning time for PI-based aerogels held over the flame of an alcohol lamp; (c) thermal conductivity of PI-based aerogels; (d) infrared camera images of PszmPIFA2 on a 350.0 °C heating platform for 30 min; (e) stress–strain plots of PszmPIFA2 during loading–unloading processes with gradient ascent strain; (f) stress–strain plots of PIFA-2.0 and PszmPIFA2 for the first compressive cycle.

Fig. 7(e) presents the stress–strain curves of a PszmPIFA (taking PszmPIFA2 as an example) at a maximum compression strain of 20%, 30%, 40%, and 50%. As can be seen, the maximum stress of PszmPIFA2 ranged from 36 to 224 kPa with an increase in strain amplitude. Furthermore, the compressive stress of PszmPIFA2 at 50% reached 224 kPa, which was 18.5% higher than that of PIFA2.0 (Fig. 7(f)). Thus, enhanced mechanical performance was induced by polysilazane modification, as the polysilazane wrapped around the junctions in the PI-based aerogels.

### 3.7. Combustion behavior of PI-based aerogels

Although PI is one of the most well-known thermostable polymer materials, it loses its mechanical properties within quite a short time when exposed to a rather high temperature in air. During the combustion experiments (Fig. 8(a)), no fume or fire was released from the PI-based aerogels (PIFAs and PszmPIFAs) when the ignition source was removed, which demonstrates their self-

extinguishing behavior. As shown in Fig. 8(b), when PIFA-2.0 was exposed to the alcohol flame, it deformed within several seconds and suffered from a severe volume shrinkage of almost 40% during the combustion process. In comparison, PszmPIFA2 maintained its shape without visible shrinkage or deformation during 60 s of combustion (Fig. 8(c)).

The high-temperature resilience and retardancy of PszmPIFA2 were further investigated by *in situ* compression in the flame of an alcohol lamp (~700 °C). As demonstrated in Figs. 8(d) and (e), PszmPIFA2 exhibited good elastic resilience during for a total of compression cycles without structural collapse and ignition upon flame burning, in comparison with the PIFA-2.0, which suffered from severe collapse and shrinkage, and turned into a compact bulk. Further investigation by SEM indicated that the cellular structure of PszmPIFA2 remained, while the honeycomb structure of the PIFA-2.0 was compressed into a dense lamellar structure (see SEM images in Figs. 8(d) and (e)). These results demonstrate that PszmPIFAs can serve as lightweight and tough insulators that are



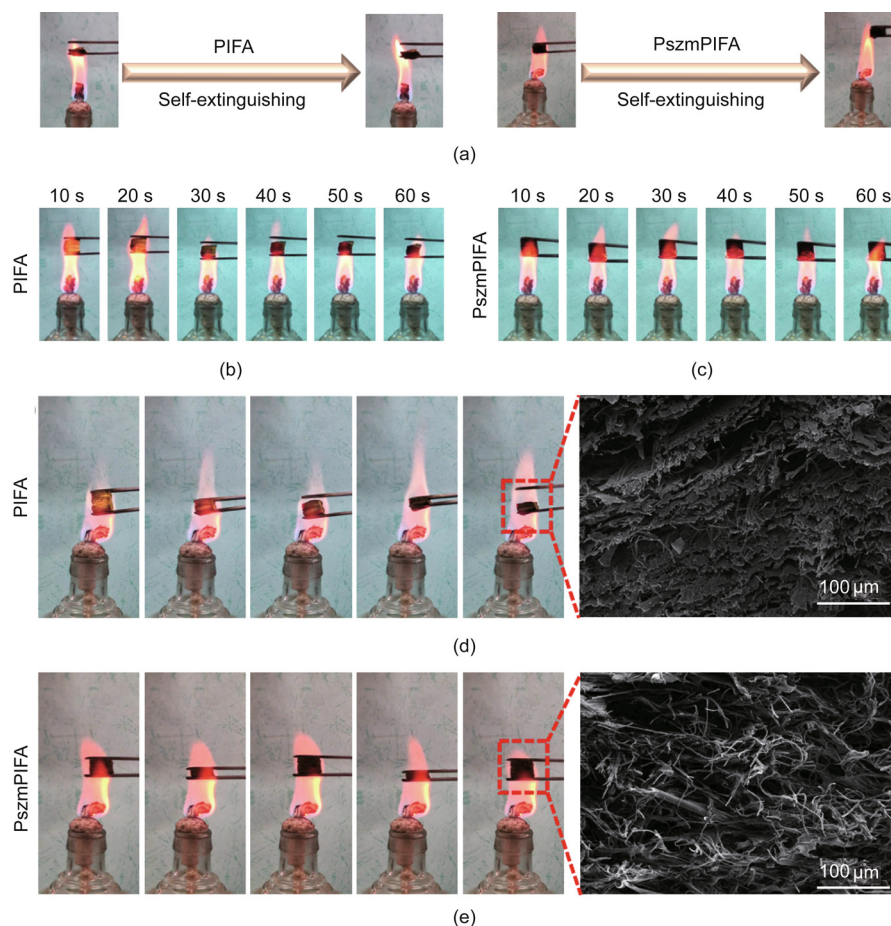


**Fig. 8.** (a) The self-extinguishing behavior of PIFAs and PszmPIFAs; (b, c) volume variation of (b) PIFA-2.0 and (c) PszmPIFA2 when exposed to the flame of an alcohol lamp for 60 s; (d, e) compression-recovery behavior of (d) PIFA-2.0 and (e) PszmPIFA2 in the flame of an alcohol lamp with their SEM images after pressing and releasing with burning.

fireproof and heatproof for potential applications such as the construction industry or insulation layers in the aerospace and aviation industries.

#### 4. Conclusions

In summary, a facile freeze-extraction method followed by VD was developed to successfully prepare PIFAs using short electro-spun PI fibers as a supporting skeleton. The proposed technique is time-, energy-, and cost-saving, as it does not involve special drying methods, in comparison with the two traditional drying techniques, FD and SD. The precursors of the PIFAs were able to withstand the capillary pressure originating from the polar solvent, making drying possible under regular vacuum conditions. The PIFAs that were obtained after imidization exhibited low density ( $\leq 52.8 \text{ mg}\cdot\text{cm}^{-3}$ ) and high porosity ( $> 96\%$ ). The PIFAs also possessed excellent mechanical properties and thermal stability. Moreover, they exhibited a good thermal insulating performance due to their high porosity and interconnected networks. Modification by coating the PIFAs with polysilazane significantly improved their fire resistance. We believe that the freezing-extraction/VD strategy can be extended to other material systems. With this facile and low-cost method, PIFAs and their composites are promising candidates for practical applications, such as lightweight building, thermal insulating, and fireproof layers for the construction and aviation industries, and high-temperature reaction catalyst carriers. In addition, by modifying the freezing and solvent-extraction setups, such as by using a larger tank and stirrer

or by using a reversible moving conveyor, the novel freezing-extraction/VD technique proposed in this work could be successfully applied for the production of large samples.

#### Acknowledgments

This work was financially supported by the National Natural Science Foundation of China (21975111, 21774053, and 51903123), and Advanced Analysis and Testing Center of Nanjing Forestry University.

#### Appendix A. Supplementary data

Supplementary data to this article can be found online at <https://doi.org/10.1016/j.eng.2021.08.024>.

#### References

- [1] Chen Y, Zhang L, Yang Y, Pang B, Xu W, Duan G, et al. Recent progress on nanocellulose aerogels: preparation, modification, composite fabrication, applications. *Adv Mater* 2021;33(11):2005569.
- [2] Chen Y, Yang Y, Xiong Y, Zhang L, Xu W, Duan G, et al. Porous aerogel and sponge composites: assisted by novel nanomaterials for electromagnetic interference shielding. *Nano Today* 2021;38:101204.
- [3] Si Y, Yu J, Tang X, Ge J, Ding B. Ultralight nanofibre-assembled cellular aerogels with superelasticity and multifunctionality. *Nat Commun* 2014;5(1):5802.
- [4] Zhang D, Cai J, Xu W, Dong Q, Li Y, Liu G, et al. Synthesis, characterization and adsorption property of cellulose nanofiber-based hydrogels. *J For Eng* 2019;4(2):92–8. Chinese.
- [5] Jiang S, Agarwal S, Greiner A. Low-density open cellular sponges as functional materials. *Angew Chem Int Ed Engl* 2017;56(49):15520–38.

- [6] Zheng C, Zhu S, Lu Y, Mei C, Xu X, Yue Y, et al. Synthesis and characterization of cellulose nanofibers/polyacrylic acid-polyacrylamide double network electroconductive hydrogel. *J For Eng* 2020;5(4):93–100. Chinese.
- [7] Si Y, Wang X, Dou L, Yu J, Ding B. Ultralight and fire-resistant ceramic nanofibrous aerogels with temperature-invariant superelasticity. *Sci Adv* 2018;4(4):eaas8925.
- [8] Jiang S, Uch B, Agarwal S, Greiner A. Ultralight, thermally insulating, compressible polyimide fiber assembled sponges. *ACS Appl Mater Interfaces* 2017;9(37):32308–15.
- [9] Duan G, Jiang S, Jérôme V, Wendorff JH, Fathi A, Uhm J, et al. Ultralight, soft polymer sponges by self-assembly of short electrospun fibers in colloidal dispersions. *Adv Funct Mater* 2015;25(19):2850–6.
- [10] Zhou L, Zhou H, Li J, Tan S, Chen P, Xu Z. Preparation and properties of nanocellulose-based oil-absorbing aerogels. *J For Eng* 2019;4(1):67–73. Chinese.
- [11] Shang Q, Chen J, Yang X, Liu C, Hu Y, Zhou Y. Fabrication and oil absorbency of superhydrophobic magnetic cellulose aerogels. *J For Eng* 2019;4(6):105–11. Chinese.
- [12] Shang Q, Hu Y, Liu C, Yang X, Zhou Y. Fabrication of superhydrophobic cellulose composite aerogels for oil/water separation. *J For Eng* 2019;4(3):86–92. Chinese.
- [13] Wang L, Qiu Y, Lv H, Si Y, Liu L, Zhang Qi, et al. 3D superelastic scaffolds constructed from flexible inorganic nanofibers with self-fitting capability and tailorable gradient for bone regeneration. *Adv Funct Mater* 2019;29(31):1901407.
- [14] Xu T, Ding Y, Wang Z, Zhao Y, Wu W, Fong H, et al. Three-dimensional and ultralight sponges with tunable conductivity assembled from electrospun nanofibers for a highly sensitive tactile pressure sensor. *J Mater Chem C* 2017;5(39):10288–94.
- [15] Si Y, Wang X, Yan C, Yang L, Yu J, Ding B. Ultralight biomass-derived carbonaceous nanofibrous aerogels with superelasticity and high pressure-sensitivity. *Adv Mater* 2016;28(43):9512–8.
- [16] Guo H, Chen Y, Li Y, Zhou W, Xu W, Pang L, et al. Electrospun fibrous materials and their applications for electromagnetic interference shielding: a review. *Compos Part A Appl Sci Manuf* 2021;143:106309.
- [17] Chen Y, Zhang L, Mei C, Li Y, Duan G, Agarwal S, et al. Wood-inspired anisotropic cellulose nanofibril composite sponges for multifunctional applications. *ACS Appl Mater Interfaces* 2020;12(31):35513–22.
- [18] Zou Y, Zhao J, Zhu J, Guo X, Chen P, Duan G, et al. A mussel-inspired polydopamine-filled cellulose aerogel for solar-enabled water remediation. *ACS Appl Mater Interfaces* 2021;13(6):7617–24.
- [19] Deuber F, Mousavi S, Federer L, Hofer M, Adlhart C. Exploration of ultralight nanofiber aerogels as particle filters: capacity and efficiency. *ACS Appl Mater Interfaces* 2018;10(10):9069–76.
- [20] Qian Z, Wang Z, Chen Yi, Tong S, Ge M, Zhao N, et al. Superelastic and ultralight polyimide aerogels as thermal insulators and particulate air filters. *J Mater Chem A* 2018;6(3):828–32.
- [21] Zhao X, Yang F, Wang Z, Ma P, Dong W, Hou H, et al. Exploration of the electrical conductivity of double-network silver nanowires/polyimide porous low-density compressible sponges. *Compos Part B Eng* 2020;182:107624.
- [22] Jiang S, Reich S, Uch B, Hu P, Agarwal S, Greiner A. Exploration of the electrical conductivity of double network silver nanowires-polyimide porous low density compressible sponges. *ACS Appl Mater Interfaces* 2017;9(39):34286–93.
- [23] Jiang S, Cheong JY, Nam JS, Kim ID, Agarwal S, Greiner A. High-density fibrous polyimide sponges with superior mechanical and thermal properties. *ACS Appl Mater Interfaces* 2020;12(16):19006–14.
- [24] Ren RP, Wang Z, Ren J, Lv YK. Highly compressible polyimide/graphene aerogel for efficient oil/water separation. *J Mater Sci* 2019;54(7):5918–26.
- [25] Cheong JY, Benker L, Zhu J, Youn DY, Hou H, Agarwal S, et al. Generalized and feasible strategy to prepare ultra-porous, low density, compressible carbon nanoparticle sponges. *Carbon* 2019;154:363–9.
- [26] Shen Y, Wang L, Liu F, Liu H, Li D, Liu Q, et al. Solvent vapor strengthened polyimide nanofiber-based aerogels with high resilience and controllable porous structure. *ACS Appl Mater Interfaces* 2020;12(47):53104–14.
- [27] Pantoja M, Boynton N, Cavicchi KA, Dosa B, Cashman JL, Meador MAB. Increased flexibility in polyimide aerogels using aliphatic spacers in the polymer backbone. *ACS Appl Mater Interfaces* 2019;11(9):9425–37.
- [28] Yuan Z, Lin H, Qian X, Shen J. Converting a dilute slurry of hollow tube-like papermaking fibers into dynamic hydrogels. *J Bioresour Bioprod* 2019;4(4):214–21.
- [29] Jiang Q, Liao X, Yang J, Wang G, Chen J, Tian C, et al. A two-step process for the preparation of thermoplastic polyurethane/graphene aerogel composite foams with multi-stage networks for electromagnetic shielding. *Compos Commun* 2020;21:100416.
- [30] Guo L, Zhang Z, Li M, Kang R, Chen Y, Song G, et al. Extremely high thermal conductivity of carbon fiber/epoxy with synergistic effect of MXenes by freeze-drying. *Compos Commun* 2020;19:134–41.
- [31] Han X, Wang Z, Ding L, Chen L, Wang F, Pu J, et al. Water molecule-induced hydrogen bonding between cellulose nanofibers toward highly strong and tough materials from wood aerogel. *Chin Chem Lett* 2021;32(10):3105–8.
- [32] Miao X, Lin J, Bian F. Utilization of discarded crop straw to produce cellulose nanofibrils and their assemblies. *J Bioresour Bioprod* 2020;5(1):26–36.
- [33] Wang Z, Dai Z, Wu J, Zhao N, Xu J. Vacuum-dried robust bridged silsesquioxane aerogels. *Adv Mater* 2013;25(32):4494–7.
- [34] Li C, Qiu L, Zhang B, Li D, Liu CY. Robust vacuum-/air-dried graphene aerogels and fast recoverable shape-memory hybrid foams. *Adv Mater* 2016;28(7):1510–6.
- [35] Yu ZL, Li GC, Fechner N, Yang N, Ma ZY, Wang X, et al. Polymerization under hypersaline conditions: a robust route to phenolic polymer-derived carbon aerogels. *Angew Chem Int Ed Engl* 2016;55(47):14623–7.
- [36] Lee J, Chang JY. Preparation of a compressible and hierarchically porous polyimide sponge via the sol-gel process of an aliphatic tetracarboxylic dianhydride and an aromatic triamine. *Chem Commun* 2016;52(68):10419–22.
- [37] Yang G, Ning T, Zhao W, Deng W, Liu X. Robust ambient pressure dried polyimide aerogels and their graphene oxide directed growth of 1D–2D nanohybrid aerogels using water as the only solvent. *RSC Adv* 2017;7(26):16210–6.
- [38] Xu X, Zhang Q, Yu Y, Chen W, Hu H, Li H. Naturally dried graphene aerogels with superelasticity and tunable Poisson's ratio. *Adv Mater* 2016;28(41):9223–30.
- [39] Yang H, Li Z, Lu B, Gao J, Jin X, Sun G, et al. Reconstruction of inherent graphene oxide liquid crystals for large-scale fabrication of structure-intact graphene aerogel bulk toward practical applications. *ACS Nano* 2018;12(11):11407–16.
- [40] Yang H, Zhang T, Jiang M, Duan Y, Zhang J. Ambient pressure dried graphene aerogels with superelasticity and multifunctionality. *J Mater Chem A* 2015;3(38):19268–72.
- [41] Yang H, Li Z, Sun G, Jin X, Lu B, Zhang P, et al. Superplastic air-dryable graphene hydrogels for wet-press assembly of ultrastrong superelastic aerogels with infinite macroscale. *Adv Funct Mater* 2019;29(26):1901917.
- [42] Liao X, Hu P, Agarwal S, Greiner A. Impact of the fiber length distribution on porous sponges originating from short electrospun fibers made from polymer yarn. *Macromol Mater Eng* 2020;305(2):1900629.
- [43] Fan W, Zuo L, Zhang Y, Chen Y, Liu T. Mechanically strong polyimide/carbon nanotube composite aerogels with controllable porous structure. *Compos Sci Technol* 2018;156:186–91.
- [44] Fan W, Zhang X, Zhang Yi, Zhang Y, Liu T. Lightweight, strong, and super-thermal insulating polyimide composite aerogels under high temperature. *Compos Sci Technol* 2019;173:47–52.
- [45] Zhao X, Yang F, Wang Z, Ma P, Dong W, Hou H, et al. Mechanically strong and thermally insulating polyimide aerogels by homogeneity reinforcement of electrospun nanofibers. *Compos Part B Eng* 2020;182:107624.
- [46] Zhu Z, Yao H, Wang F, Dong J, Wu K, Cao J, et al. Fiber reinforced polyimide aerogel composites with high mechanical strength for high temperature insulation. *Macromol Mater Eng* 2019;304(5):1800676.
- [47] Qian Z, Yang M, Li R, Li D, Zhang J, Xiao Y, et al. Fire-resistant, ultralight, superelastic and thermally insulated polybenzazole aerogels. *J Mater Chem A* 2018;6(42):20769–77.
- [48] Song J, Chen C, Yang Z, Kuang Y, Li T, Li Y, et al. Highly compressible, anisotropic aerogel with aligned cellulose nanofibers. *ACS Nano* 2018;12(1):140–7.
- [49] Jia C, Li L, Liu Y, Fang B, Ding H, Song J, et al. Highly compressible and anisotropic lamellar ceramic sponges with superior thermal insulation and acoustic absorption performances. *Nat Commun* 2020;11(1):3732.
- [50] Xie C, He L, Shi Y, Guo ZX, Qiu T, Tuo X. From monomers to a lasagna-like aerogel monolith: an assembling strategy for aramid nanofibers. *ACS Nano* 2019;13(7):7811–24.
- [51] Zhang X, Li W, Song P, You B, Sun G. Double-cross-linking strategy for preparing flexible, robust, and multifunctional polyimide aerogel. *Chem Eng J* 2020;381:122784.
- [52] Jiang S, Reich S, Uch B, Hu P, Agarwal S, Greiner A. Exploration of the electrical conductivity of double-network silver nanowires/polyimide porous low-density compressible sponges. *ACS Appl Mater Interfaces* 2017;9(39):34286–93.
- [53] Tang Q, Fang Lu, Guo W. Effects of bamboo fiber length and loading on mechanical, thermal and pulverization properties of phenolic foam composites. *J Bioresour Bioprod* 2019;4(1):51–9.
- [54] Li J, Yu J, Wang Y, Zhu J, Hu Z. Intercalated montmorillonite reinforced polyimide separator prepared by solution blow spinning for lithium-ion batteries. *Ind Eng Chem Res* 2020;59(28):12879–88.
- [55] Wang YY, Zhou ZH, Zhou CG, Sun WJ, Gao JF, Dai K, et al. Lightweight and robust carbon nanotube/polyimide foam for efficient and heat-resistant electromagnetic interference shielding and microwave absorption. *ACS Appl Mater Interfaces* 2020;12(7):8704–12.
- [56] Liu W, Luo Y, Xu C. A new organosilicon adhesive based on polysiloxane and polysilazane. *High Perform Polym* 2013;25(5):543–50.
- [57] Barroso G, Döring M, Horcher A, Kienzle A, Motz G. Polysilazane-based coatings with anti-adherent properties for easy release of plastics and composites from metal molds. *Adv Mater Interfaces* 2020;7(10):1901952.
- [58] Gardelle B, Duquesne S, Vu C, Bourbigot S. Thermal degradation and fire performance of polysilazane-based coatings. *Thermochim Acta* 2011;519(1–2):28–37.
- [59] Ricci PC, Gulleri G, Fumagalli F, Carbonaro CM, Corpino R. Optical characterization of polysilazane based silica thin films on silicon substrates. *Appl Surf Sci* 2013;265:470–4.